

On Timing Properties of LYSO-based Calorimeters

D. Anderson¹, A. Apresyan¹, A. Bornheim¹, J. Duarte¹,
C. Pena¹, A. Ronzhin², M. Spiropulu¹, J. Trevor¹, and S. Xie¹

¹*California Institute of Technology, Pasadena, CA, USA*

²*Fermi National Accelerator Laboratory, Batavia, IL, USA*

Abstract

We present Test Beam studies and results on the timing performance and characterization of the time resolution of LYSO-based calorimeters. We demonstrate time resolution of 30 ps is achievable for a particular design. We discuss precision timing calorimetry as a tool for mitigation of physics object performance degradation effects due to the large number of simultaneous interactions in the high luminosity environment foreseen at the Large Hadron Collider.

1 Introduction

The high luminosity upgrade of the Large Hadron Collider (HL-LHC) at CERN [1] is expected to provide instantaneous luminosities of $5 \times 10^{34} \text{ cm}^{-2}\text{s}^{-1}$. The enhanced data rates will provide the datasets necessary to perform precision measurements of the Higgs couplings, probe rare Higgs processes, study the scattering of longitudinally polarized W bosons and search for physics beyond the standard model.

The rate of simultaneous interactions per bunch crossing (pileup) is projected to reach an average of 140 to 200. The large amount of pileup increases the likelihood of confusion in the reconstruction of events of interest, due to the contamination from particles produced in different pileup interactions. The ability to discriminate between

27 jets produced in the events of interests – especially those associated
28 with the vector boson fusion processes – and jets produced by pileup
29 interactions will be degraded, the missing transverse energy resolution
30 will deteriorate, and several other physics objects performance metrics
31 will suffer.

32 One way to mitigate pileup confusion effects, complementary to
33 precision tracking methods, is to perform a time of arrival measure-
34 ment associated with a particular layer of the calorimeter, allowing
35 for a time assignment for both charged particles and photons. Such
36 a measurement with a precision of about 20 to 30 ps, when unam-
37 biguously associated to the corresponding energy measurement, will
38 significantly reduce the inclusion of pileup particles in the reconstruc-
39 tion of the event of interest given that the spread in collision time
40 of pileup interactions is about 200 ps. The association of the time
41 measurement to the energy measurement is crucial, leading to a pro-
42 totype design that calls for the time and energy measurements to be
43 performed in the same active detector element. It is in this context
44 that we study the possibility of measuring the time of arrival of par-
45 ticles with a calorimetric device.

46 We focus our studies on measurements of the time of flight using
47 sampling calorimeters based on LYSO crystals. Due to its very high
48 light yield ($\sim 30\text{K}$ photons/MeV) [2], and radiation tolerance [3–6],
49 LYSO is the active element of one of the options considered for the
50 upgrade of the Compact Muon Solenoid (CMS) detector for the HL-
51 LHC [7].

52 In Figure 1 we present a simplified illustration of the major time
53 scales associated to the timing measurement using a monolithic crys-
54 tal calorimeter. Upon entering the crystal the photon or electron
55 travels at the speed of light, interacts, and begins to shower, produc-
56 ing scintillation light in the crystal. The time between the entry of
57 the photon into the crystal and the first interaction is denoted by t_I
58 and for high energy impinging particles it is the shower development
59 time. The time associated with the conversion of the incident photon
60 to scintillation light is denoted by t_S . The scintillation light travels
61 from the point of interaction to the photodetector at the velocity c/\hat{n} ,
62 where \hat{n} is the effective index of refraction of the crystal [8]. The
63 time associated with the propagation of the scintillation light to the
64 photodetector is denoted by t_P . Once the scintillation light reaches
65 the photodetector, the photons are converted into an electrical signal.
66 The time associated with this process is known as the photodetector

67 signal transit time, t_T . Finally, the data acquisition (DAQ) system
 68 has a characteristic time constant t_D . Each of these time intervals
 69 will fluctuate or jitter on an event-by-event basis, contributing to the
 70 time resolution.

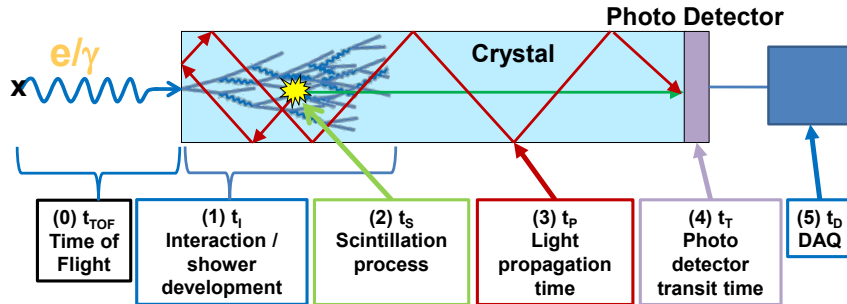


Figure 1: Timing measurement schematic breakdown using a monolithic, large scintillating crystal. The incident particle impinges on the crystal face from the left. The characteristic time intervals are discussed in the text.

71 Previous studies [9], measured the time resolution at different ab-
 72 sorber thickness for electron beams with energies varying from 12 to
 73 32 GeV, and showed that the time of arrival of the front of an elec-
 74 tromagnetic shower can be determined with a precision better than
 75 20 ps. The electronic time resolution of the DAQ system was mea-
 76 sured to be about 6 ps. Using the same techniques, we measure the
 77 time resolution of the MCP-PMT photodetectors used in the studies
 78 presented in this paper to be between 11 ps and 14 ps, depending on
 79 the exact device.

80 To characterize the time resolution of an inorganic crystal scin-
 81 tillator calorimeter we study the contributions due to fluctuations in
 82 the shower development, scintillation process, and light propagation
 83 to the photodetector. We take advantage of the very large number of
 84 scintillation photons in a LYSO crystal which result in modest fluc-
 85 tuations associated with the creation and transit of each particular
 86 scintillation photon for a LYSO-based detector.

87 2 Experimental Setup

88 A schematic diagram of a typical time of flight measurement setup is
 89 shown in Figure 2. All measurements involve a fast photodetector,

90 typically a micro-channel-plate photo-multiplier-tube (MCP-PMT),
 91 which measures the reference (t_0) timestamp, and a photodetector
 92 further downstream that detects the signal associated with the elec-
 93 tronagnetic shower and provides a simultaneous energy and time (t_1)
 94 measurement.

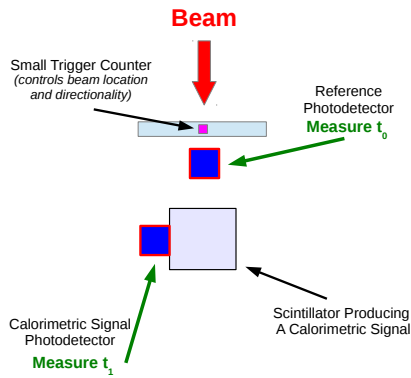


Figure 2: The basic schematic diagram of the experimental setup for a typical time of flight measurement is shown to illustrate the basic detector elements. One photodetector is used as a time reference and the second measures energy and time simultaneously.

95 In our study we used two types of MCP-PMT photodetectors, one
 96 produced by Hamamatsu (model R3809-52) [10], and one produced by
 97 Photek (model PMT240) [11]. A DRS4 waveform digitizer V4 eval-
 98 uation board [12] was used as the primary DAQ system, connected
 99 to a laptop via USB interface. The DRS chip contains a switched ca-
 100 pacitor array (SCA) with 1024 cells, capable of digitizing eight analog
 101 signals with high speed (5 GSPS) and high accuracy (11.5 bit SNR).
 102 All experimental beam studies were performed at the Fermilab Test
 103 Beam Facility (FTBF), which provided proton beams from the Fer-
 104 milab Main Injector accelerator at 120 GeV, and secondary electron
 105 beams of energies ranging from 4 to 32 GeV. All detector elements
 106 were placed inside of a dark box lined with copper foil, providing RF
 107 shielding. A $2 \times 2 \text{ mm}^2$ scintillator was placed inside the box at the
 108 upstream extremity and used to trigger the DAQ readout, provid-
 109 ing a strict constraint on the location and directionality of the beam

110 particles used in the time of flight studies. A differential Cherenkov
111 counter (not shown in the schematic) provided by the FTBF facility
112 and located upstream of our experimental hall, was used for electron
113 identification.

114 3 Event Selection and Data Analysis

115 Our primary target is to reconstruct the time of flight of beam parti-
116 cles between different detector elements. Different time reconstruction
117 algorithms are used for different detector elements, and all involve the
118 assignment of a timestamp using specific features of each correspond-
119 ing signal pulse. The signal pulse for the reference time detector is
120 very sharp and symmetric around its maximum amplitude, as shown
121 in Figure 3. Hence for the reference detector we determine the time
122 position of the pulse peak by fit a Gaussian function to the peak of
123 the pulse, using three sampling points before the pulse maximum and
124 four sampling points after. The fitted mean parameter of the Gaus-
125 sian function is assigned as the timestamp t_0 . The signal pulse for the
126 downstream time measurement is the result of scintillation light, and
127 exhibits a fast rising edge and a significantly slower decay. Therefore,
128 we assign the timestamp t_1 using a constant fraction of the rising edge.
129 A linear function is fit to the sampling points between 10% and 60%
130 of the pulse maximum and the timestamp is assigned as the time at
131 which the fitted linear function rises to 20% of the pulse maximum.
132 Examples of fits performed to assign a time stamp from each pulse
133 are shown in Figure 4. The impact from the choice of the functional
134 forms is studied by using a set of alternative functions in the fits, and
135 choosing the one that results in the best time resolution. Among the
136 functions that we tested, the difference between the best and worst
137 performing functions was about 8 psec.

138 Event selection and pulse cleaning procedures are used to eliminate
139 abnormal pulses in the readout, as described in [9]. Large signals
140 above 500 mV are rejected because they saturate the DRS4 inputs.
141 Only pulses with amplitude larger than 20 mV are used for time of
142 flight measurements, in order to reduce the impact of noise from the
143 DRS waveform digitizer DAQ system. Events containing more than
144 one pulse within the 200 ns readout window are not used. Attenuators
145 were used to extend the dynamic range of the DRS4 waveform digitizer
146 in cases when a large fraction of signal pulses are saturated.

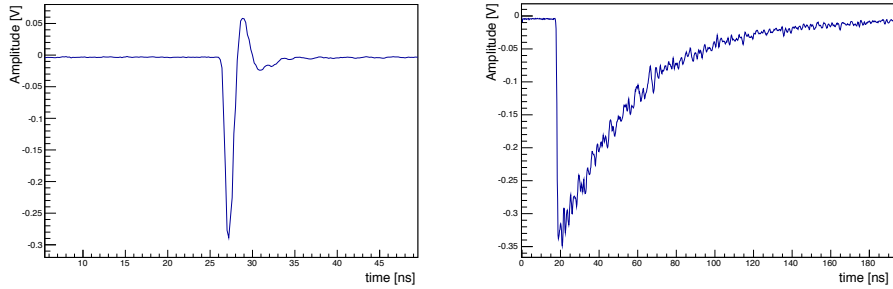


Figure 3: Sample pulses as digitized by the DRS4 board. On the left a pulse is shown from the reference Hamamatsu R3809 MCP-PMT, and on the right is a pulse from the Hamamatsu R3809 MCP-PMT optically coupled to a $(1.7 \text{ cm})^3$ LYSO crystal cube recorded using 8 GeV electron beam.

147 4 Timing in LYSO-based Calorimeters

148
149
150
151
152
153
154
155
156
157
158
The timing measurement in LYSO-based calorimeters is driven by
three main factors – other than the intrinsic transit time of the pho-
todiector itself and the DAQ electronics : a) the shower profile fluc-
tuations, b) the scintillation time, and c) the light propagation time.
Stochastic processes during the development of an electromagnetic
shower affect the time of observed signals, as both the transverse size
and the depth of the shower can fluctuate event-by-event. Random
processes in the scintillation mechanism and the randomization of the
optical paths for the scintillation light affect both the speed of the
signal formation and the time jitter. We study these effects using two
independent experimental setups.

159
160
161
162
163
164
165
166
167
For a homogeneous crystal calorimeter we are interested in the
characterization and optimization of the light propagation time, i.e.
the time the scintillation light travels down the length of the crystal.
Our setup uses a small LYSO cube with linear dimensions of 17mm
as the active scintillation element. The size of this element reduces
the effect of the light propagation time and jitter. The LYSO cube
is placed behind about $4.5 X_0$ radiation lengths of lead. Using this
LYSO-based sampling calorimeter, we measure the time resolution of
electrons.

168
169
170
We also study a shashlik calorimeter composed of alternating layers
of tungsten and LYSO, in which scintillation light is extracted through
wavelength shifting (WLS) fibers. In this setup, the light propagation

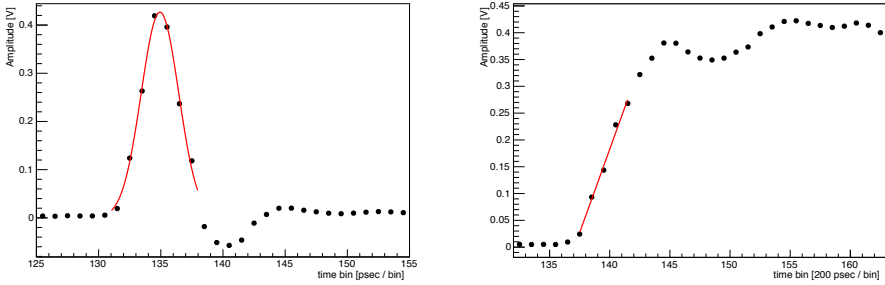


Figure 4: Sample fits used to assign timestamps to digitized MCP-PMT pulses. On the left is a pulse from the reference Hamamatsu R3809 MCP-PMT, and on the right is a pulse from the Hamamatsu R3809 MCP-PMT optically coupled to a $(1.7 \text{ cm})^3$ LYSO crystal recorded during an 8 GeV electron run.

171 time through the fiber is the dominant factor of the timing measurement.
 172 We study as a baseline an alternate version of this calorimeter
 173 where the light is extracted through direct optical coupling of the photo-
 174 todetectors at the edges of a few LYSO layers to minimize the light
 175 propagation time.

176 4.1 Timing Studies of the LYSO-based Sam- 177 pling Calorimeter

178 We study the combined impact of the shower profile fluctuations, the
 179 scintillation mechanism in LYSO, and the light propagation time res-
 180 olution using a sampling calorimeter with a $(1.7 \text{ cm})^3$ LYSO cube
 181 as active element. The LYSO crystal is wrapped in Tyvek and at-
 182 tached to the Hamamatsu R3809 MCP-PMT (HAMB) with opti-
 183 cal coupling [13]. A second Hamamatsu MCP-PMT photodetector
 184 (HAMA) is placed upstream of the calorimeter and is used to mea-
 185 sure the reference time. A schematic diagram and a photograph of
 186 the experimental setup are shown in Figure 5.

187 To ensure that the electron beam is constrained to within a $2 \times$
 188 2 mm^2 region, a plastic scintillator placed upstream and approxi-
 189 mately 2 mm by 2 mm in cross sectional area is used to trigger the
 190 DAQ readout on the DRS digitizer. Electron events are identified by
 191 requiring a signal with amplitude larger than 10 mV in a Cherenkov
 192 counter located upstream. Large lead bricks are placed upstream of
 193 the Hamamatsu R3809 MCP-PMT (HAMB), out of the path of the

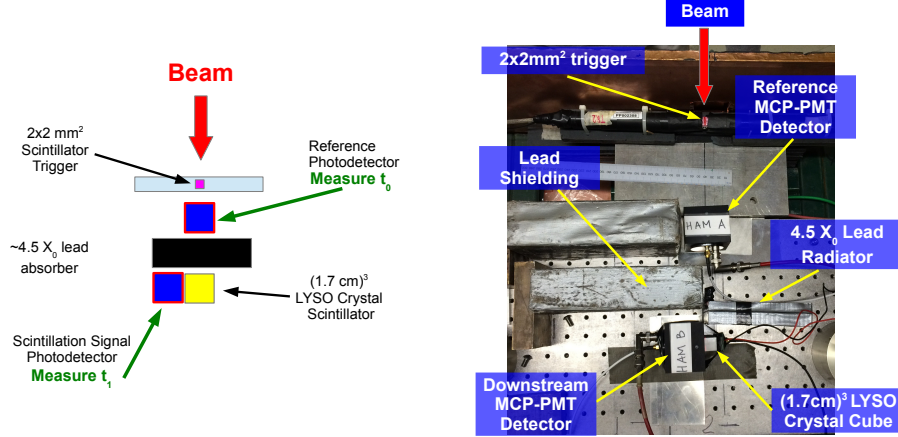


Figure 5: A schematic diagram of the experimental setup for the time of flight measurement using the LYSO sampling calorimeter is shown on the left, along with a picture of the experimental setup shown on the right.

beam. These shield the photodetector from stray particles produced in events where an electromagnetic shower occurs upstream of the lead radiator. Such stray shower particles yield very fast signals which can significantly contaminate the scintillation signal. Using the same experimental setup without the LYSO active element in place, we find that stray shower type events yield less than 10% contamination and give a negligible effect on the scintillation signal.

The thickness of the LYSO active element is relatively small and captures only a fraction of the total energy of the electron, but yields a reasonable energy measurement as it is close to the shower maximum.

The time of flight measurement is performed using the LYSO sampling calorimeter for electron beams with energies varying from 4 GeV to 32 GeV. The corresponding measured time of flight distributions are shown in Figure 6. We achieve the best time resolution of 34 ps for electrons with beam energy of 32 GeV.

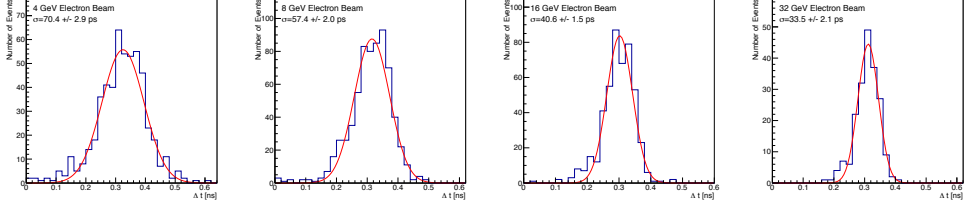


Figure 6: Time of flight distributions for the LYSO cube sampling calorimeter for 4 GeV (top left), 8 GeV (top right), 16 GeV (bottom left), 32 GeV (bottom right) electron beam energy.

209 The time resolution measurement is plotted as a function of the
 210 beam energy in Figure ?? (left). We fit the result to the sum of a $1/\sqrt{E}$
 211 term and a constant term of about 11 ps. Given that we measure the
 212 contribution to the intrinsic time resolution of the photodetector and
 213 the DAQ electronics to be about 20 ps [9], using the results from the
 214 32 GeV electron beam, we infer that the combined contribution to the
 215 time resolution from the shower profile fluctuations, the scintillation
 216 mechanism, and the light propagation time inside the LYSO cube is
 217 about 27 ps.

218 **4.2 Timing Studies of the LYSO-Tungsten Shash-
 219 lik Calorimeter**

220 **4.2.1 Wavelength shifting fibers readout (WLS Y11 &
 221 DSB1)**

222 We study the time resolution of a LYSO-tungsten Shashlik calorime-
 223 ter, one of the proposed choices for the Phase 2 upgrade of the CMS
 224 endcap calorimeter system [7]. We compare the time resolution per-
 225 formance for two alternative light propagation schemes.

226 In our setup the scintillation light is collected by WLS fibers that
 227 pass through a set of four holes in the LYSO and tungsten layers.
 228 In Figure 7, a shashlik cell and the light extraction scheme is illus-
 229 trated. A schematic diagram and a photograph showing this experi-
 230 mental setup are shown in Figure 8. Two MCP-PMTs by Hamamatsu
 231 (R3809) are used to collect the scintillation light, while a Photek 240
 232 MCP-PMT is used as a reference time detector.

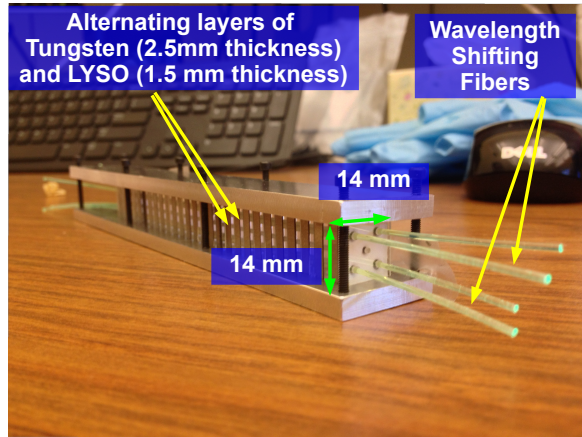


Figure 7: The shashlik configuration based upon interleaved W and LYSO layers. Twenty-eight LYSO crystal plates and twenty-seven W plates comprise the module. Four WLS fibers are used to read out the scintillation light from the tiles.

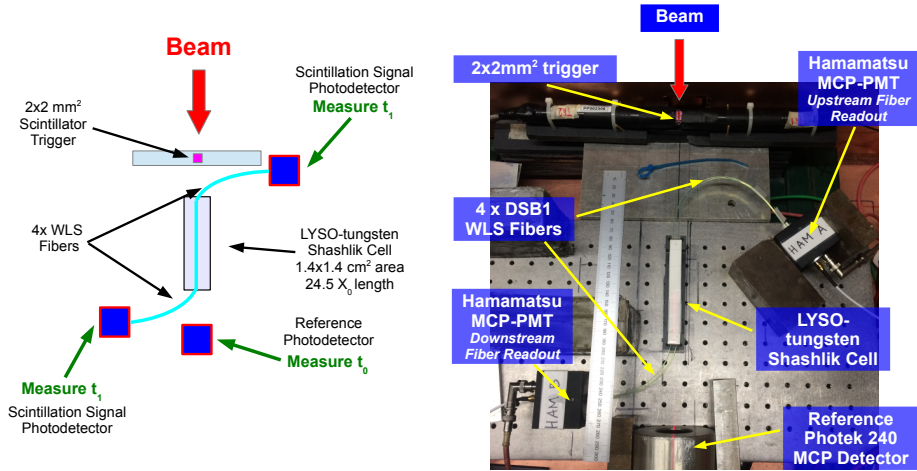


Figure 8: A schematic diagram of the experimental setup for the time of flight measurement using the LYSO-tungsten shashlik calorimeter with fiber signal extraction, along with a photograph of the experimental setup.

233 We compare the signal pulses obtained using two different types
 234 of WLS fiber in the same LYSO-tungsten shashlik calorimeter. In
 235 Figure 9 (a) and (b) and we show the pulse shapes averaged over a
 236 few hundred events obtained using DSB1 fibers [14] and Y11 fibers,
 237 plotted in blue and red respectively. We find that the rise time of the
 238 pulse obtained using the DSB1 fibers, about 2.4 ns, is significantly
 239 faster than the rise time of the pulse obtained using the Y11 fibers,
 240 which is about 7.1 ns. To optimize the time resolution of this type of
 241 calorimeter the DSB1 fiber provides a better choice than Y11 if only
 242 this parameter is considered. The signal rise times we observe are
 243 comparable to the measured decay times of the corresponding WLS
 244 fibers [14].

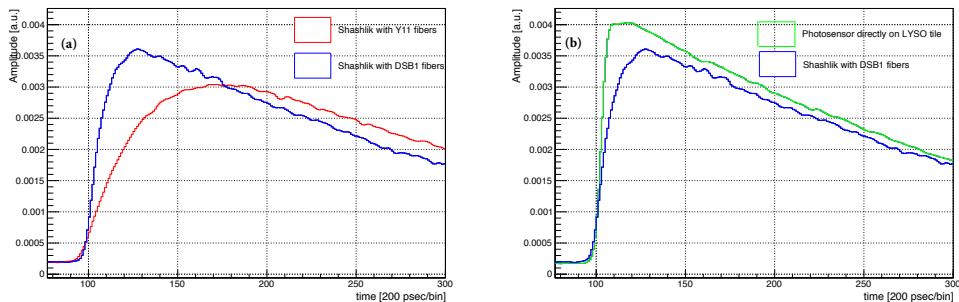


Figure 9: (a) Pulse shapes digitized by the DRS4 board and averaged over several hundred events obtained from the LYSO-tungsten shashlik calorimeter with light extracted using DSB1 (blue) and Y11 (red) WLS fibers. (b) DSB1(blue) shashlik average light pulse shape compared with the averaged pulse shape obtained from direct optical coupling of the photodetector to one edge of a LYSO tile in the shashlik calorimeter. (green)

245 Using the shashlik calorimeter cell with DSB1 fibers, we measure
 246 the time resolution for electron beams with energy varying between
 247 4 GeV and 32 GeV. In Figure 10(b) we show the distribution of the
 248 pulse integral which is proportional to the total collected charge, for
 249 the 32 GeV beam, and observe an energy resolution of about 5% while
 250 for the small LYSO cube shown in 10 (a), the energy resolution was
 251 about 20%. For this particular run in the Shashlik setup, no electron
 252 identification requirements could be made due to a misconfiguration
 253 of the upstream Cherenkov counter, so the background is visible.

254 Time of flight distributions, fitted to gaussian functions, are shown

255
 256
 257
 258
 259
 260
 261
 262

in Figure 11, and the σ parameter of the gaussian fit is plotted as a function of the beam energy in Figure 16. We find that the dependence of the time resolution on beam energy follows a $1/\sqrt{E}$ functional form, indicating that the current calorimeter setup remains in the photostatistics limited regime. The best time resolution we obtain with this setup is 104 ps. As the measurements are photostatistics limited, the result can be improved in the future if the light collection efficiency is increased.

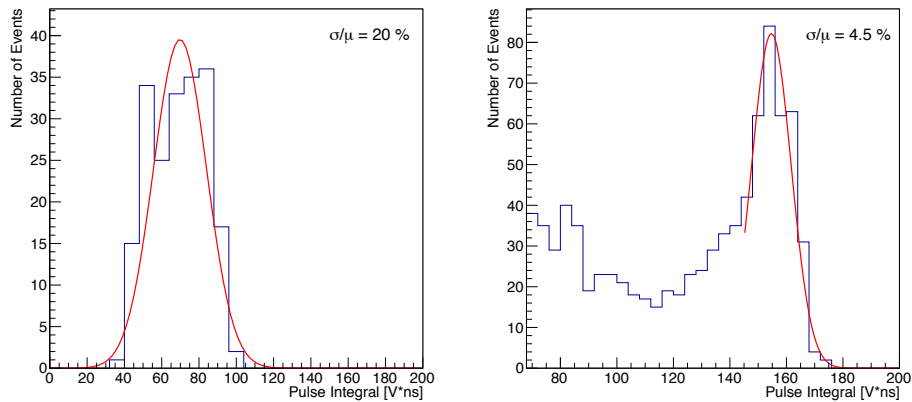


Figure 10: (Left) Histogram of the pulse integral which is proportional to the total collected charge is shown for events recorded using the LYSO cube sampling calorimeter for a 32 GeV electron beam. (Right) Histogram of the pulse integral for events recorded using the LYSO-tungsten shashlik calorimeter using DSB1 fibers, for a 32 GeV electron beam. The background is included due to a misconfiguration of the Cherenkov counter.

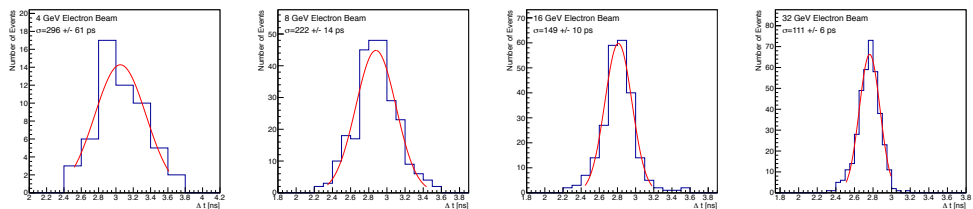


Figure 11: Time of flight distributions for the LYSO-tungsten shashlik calorimeter using DSB1 fibers for electron beams with varying beam energies.

263 **4.2.2 Directly coupled MCP-PMTs to LYSO shashlik**
 264 **plates**

265 In this setup the MCP-PMT photodetectors are directly coupled to
 266 the edges of two adjacent LYSO layers in the shashlik calorimeter and
 267 scintillation light is directly transported to the photodetector through
 268 the edges of the tile layers. A schematic diagram and corresponding
 269 picture of the experimental setup are shown in Figure 12. In Figure 13,
 270 we show a zoomed-in photograph of the exposed LYSO plates from
 271 which the scintillation light signal is extracted.

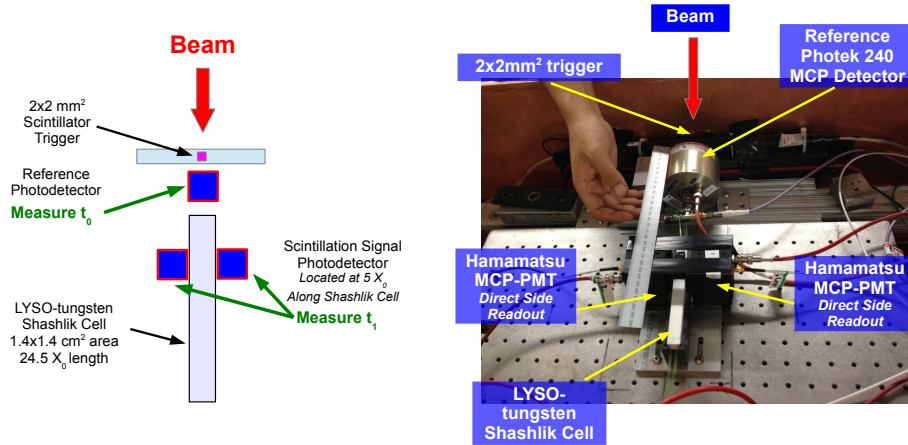


Figure 12: A schematic diagram of the experimental setup for the time of flight measurement using the LYSO-tungsten shashlik calorimeter with signal extraction from the edges of two LYSO plates, along with a picture of the experimental setup.

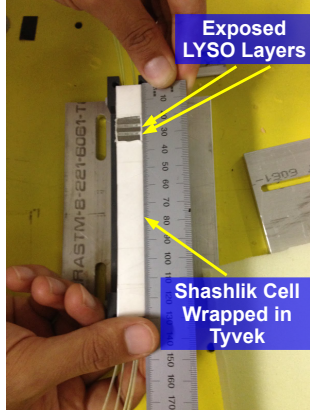


Figure 13: A photograph of the two exposed LYSO layers in the shashlik cell. The scintillation light signal is extracted by optically coupling the edges of these two exposed LYSO layers to MCP-PMT photodetectors.

With this setup we invoke an interplay between the light propagation jitter and the limited photostatistics. By placing the photodetectors in direct contact with the edges of two LYSO layers, we minimize the distance the scintillation light travels to reach the photodetectors, and reduce the impact of light propagation jitter on the time measurement resolution. However in this setup we have also reduced the available photostatistics, as we collect light from only a small fraction of the shashlik cell. In Figure 14, we show the time of flight distributions for electron beams at various energies, fitted to gaussian functions. The width of the best-fit gaussian is plotted as a function of the beam energy in Figure 16. The best time resolution that we obtain is about 55 ps, and fitting the result to the sum of a $1/\sqrt{E}$ term and a constant term, we find a constant term of about 30 ps.

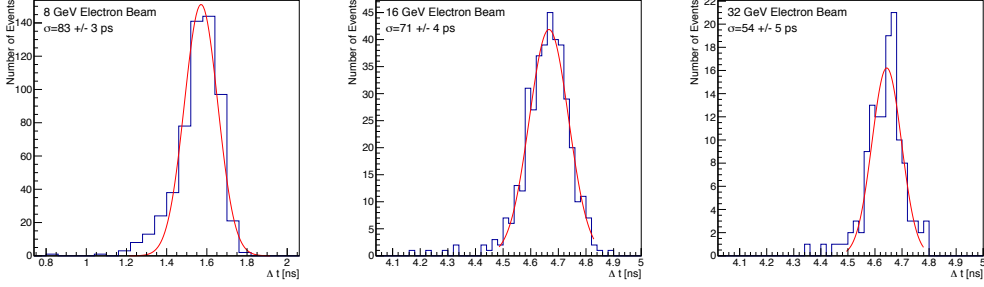


Figure 14: Time of flight distributions for the LYSO-tungsten shashlik calorimeter with signal extracted from the edges of two LYSO layers.

Figure 15:

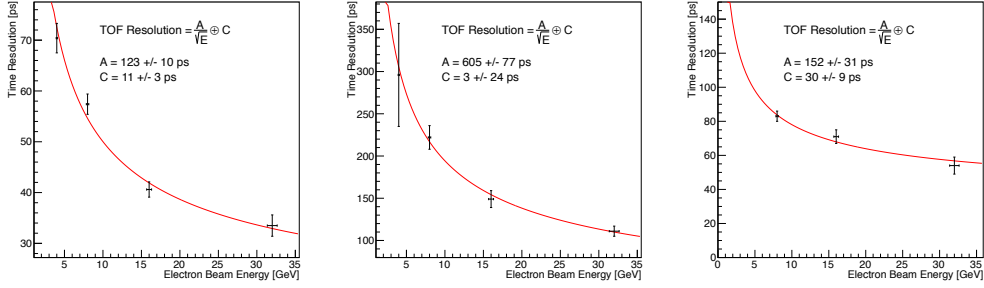


Figure 16: Timing resolution measurement as a function of the electron beam energy for (left) the LYSO cube sampling calorimeter (middle) the LYSO-tungsten shashlik calorimeter read-out with DSB1 fibers (right) the LYSO-tungsten shashlik calorimeter read-out directly by optically coupling to the edges of two LYSO layers. In all cases we fit the data with a function of $1/\sqrt{E}$ and a constant term.

285 In summary, we find that removing the impact of the wavelength
 286 shifting mechanism and minimizing the impact of optical transit does
 287 indeed improve the time resolution, but at a cost in photostatistics.
 288 Results obtained in this experiment suggest that a LYSO-tungsten
 289 shashlik calorimeter with edge readout can likely achieve 30 ps reso-
 290 lution provided some improvement to the light collection efficiency is
 291 achieved.

292

5 Results Discussion and Summary

293

294

295

296

297

298

299

300

301

302

303

304

305

306

307

308

309

310

311

312

313

314

In this article we have described studies characterizing the timing performance of LYSO-based calorimeters. Using a $(1.7\text{ cm})^3$ LYSO crystal that samples the electromagnetic showers created by electrons of various energies ranging from 4 GeV to 32 GeV at about $4.5 X_0$, we infer that the contribution to the time resolution from event-by-event fluctuations of the shower profile, the scintillation process, and the light propagation is less than 30 ps. Studies using different wavelength shifting fibers in a LYSO-tungsten shashlik calorimeter demonstrates that the choice of the fiber affects the timing performance. Besides the absorption and re-emission processes in the fibers, we found that another important factor influencing the timing performance is the light extraction efficiency. Using DSB1 fibers, despite being photostatistics limited, we obtained a best time resolution of about 100 ps. A future development of such a detector will be focused on increasing the light collection efficiency. In a setup where the scintillation light from the LYSO-tungsten shashlik calorimeter is extracted via the edges of two LYSO layers, thereby removing completely the wavelength shifting mechanism and long light propagation distance, we achieve a best time resolution of 55 ps. The result indicates that such a calorimeter design can achieve the 30 ps time resolution benchmark obtained with the LYSO cube provided some improvement to the light collection efficiency.

315

316

317

318

319

320

321

322

323

324

325

326

327

328

In comparing results using different light extraction schemes, we find that at a given light yield the time resolution depends significantly on the light propagation fluctuations. As the light yield increases the dependence on the light propagation fluctuations is reduced. The effect can be seen in the summary Figure 17 where we show the dependence of the time resolution on the average pulse height for the shashlik cell with light extracted through the DSB1 fibers and for the sampling calorimeter with the LYSO cube. For the same average pulse height of 500 mV, the LYSO cube time resolution is about half of the shashlik using the DSB1 fibers which have also twice the rise time. As the pulse height increases the time resolution improves. Extrapolating to the regime of very large light yield, we should be able to reach asymptotically the best resolution without limitations from the light propagation fluctuations.

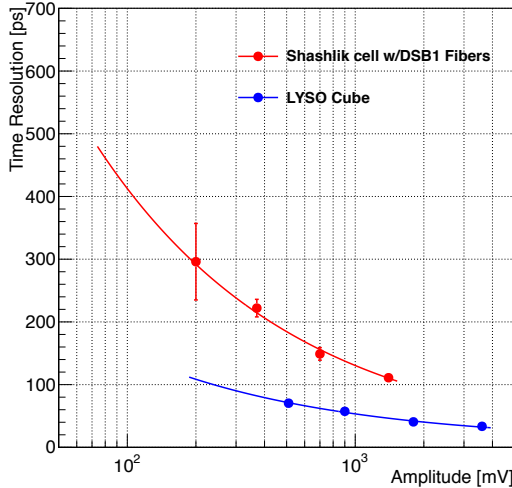


Figure 17: Comparison of time resolutions obtained with the $(1.7\text{ cm})^3$ LYSO cube (blue), and the LYSO-tungsten shashlik calorimeter with light extracted using DSB1 fibers (red). The x-axis in this figure displays the amplitude of the signal, corrected for the attenuation factors.

329 In summary, using a LYSO-based calorimeter and different light
 330 propagation experimental setups we obtain about 30 ps resolution time
 331 measurement for the maximum light yield achieved. As a follow-up
 332 we will investigate the time resolution in the limit of very large light
 333 yield, and attempt to improve the light collection efficiency in these
 334 types of detectors.

335 6 Acknowledgements

336 We would like to thank Erik Ramberg and Sergey Los for their help
 337 and support of this work, and Aria Soha and the FTBF test beam
 338 facility for the beam delivery and control. We thank Randy Ruchti
 339 for providing us with the DSB1 fibers used in the measurements, and
 340 Eileen Hahn for the high quality work in polishing the fibers. We
 341 would also like to thank Ewa Skup and Geoff Savage for help with
 342 operation of the Cherenkov counters, and to Todd Nobel for organizing
 343 and providing supporting equipment at FTBF.

344 This work is supported by funding from Fermi Research Alliance,
 345 LLC under Contract No. DE-AC02-07CH11359 with the United States

346 Department of Energy and from California Institute of Technology
347 High Energy Physics under Contract DE-SC0011925 with the United
348 States Department of Energy.

349

References

- 350 [1] L. Rossi, and O. Brüning, “High Luminosity Large Hadron
351 Collider A description for the European Strategy Preparatory
352 Group,” Tech. Rep. CERN-ATS-2012-236, CERN, Geneva, Aug
353 2012.
- 354 [2] L. Zhang, R. Mao, F. Yang, and R. Zhu, “LSO/LYSO Crystals for
355 Calorimeters in Future HEP Experiments,” *IEEE Transactions
356 on Nuclear Science*, vol. 61, pp. 483–488, Feb 2014.
- 357 [3] R. Mao, L. Zhang, and R. Zhu, “Gamma ray induced radi-
358 ation damage in PWO and LSO/LYSO crystals,” in *Nuclear
359 Science Symposium Conference Record (NSS/MIC), 2009 IEEE*,
360 pp. 2045–2049, Oct 2009.
- 361 [4] J. Chen, R. Mao, L. Zhang, and R. Zhu, “Gamma-Ray Induced
362 Radiation Damage in Large Size LSO and LYSO Crystal Sam-
363 ples,” *IEEE Transactions on Nuclear Science*, vol. 54, pp. 1319–
364 1326, Aug 2007.
- 365 [5] L. Zhang, R. Mao, and R. Zhu, “Effects of neutron irradia-
366 tions in various crystal samples of large size for future crystal
367 calorimeter,” in *Nuclear Science Symposium Conference Record
368 (NSS/MIC), 2009 IEEE*, pp. 2041–2044, Oct 2009.
- 369 [6] G. Dissertori, D. Luckey, Nessi-Tedaldi, *et al.*, “Results on dam-
370 age induced by high-energy protons in LYSO calorimeter crys-
371 tals,” *NIM A* 745 (2014) 1-6.
- 372 [7] D. Contardo and J. Spalding, “CMS Phase 2 Upgrade: Prelimi-
373 nary Plan and Cost Estimate,” Tech. Rep. CERN-RRB-2013-124,
374 CERN, Geneva, Oct 2013.
- 375 [8] W. W. Moses and S. E. Derenzo, “Prospects for Time-of-Flight
376 PET using LSO Scintillator,” *IEEE Transactions on Nuclear Sci-
377 ence*, vol. 46, pp. 474–478, June 1999.

- 378 [9] A. Ronzhin, S. Los, E. Ramberg, *et al.*, “Development of a new
379 fast shower maximum detector based on microchannel plates pho-
380 tomultipliers (MCP-PMT) as an active element,” *NIM A* **759**
381 (*2014*) 65-73.
- 382 [10] <http://www.hamamatsu.com/resources/pdf/etd/R3809U-50 TPMH1067E09.pdf>.
- 384 [11] <http://www.photek.com/pdf/datasheets/detectors/DS006 Photomultipliers.pdf>.
- 386 [12] S. Ritt, R. Dinapoli, and U. Hartmann, “Application of the DRS
387 chip for fast waveform digitizing,” *NIM A* **623** (*2010*) 486-488.
- 388 [13] <http://www.ellsworth.com/dow-corning-q2-3067-optical-couplant-453g-bottle>.
- 389 [14] M. Albrecht, K. Andert, P. Anselmino, *et al.*, “Scintillators
390 and Wavelength Shifters for the Detection of Ionizing Radia-
391 tion,” *Proceedings of the 8th Conference on astroparticle, parti-*
392 *cle and space physics, detectors and medical physics applications*,
393 pp. 502–511, 2003.